Iran J Sci Technol Trans Mech Eng (2019) 43:707–718
https://doi.org/10.1007/s40997-018-0227-0

RESEARCH PAPER

Effects of Inclined Magnetic Field on Entropy Generation in Nanofluid Over a Stretching Sheet with Partial Slip and Nonlinear Thermal Radiation

B. Ganga[1] · M. Govindaraju[2] · A. K. Abdul Hakeem[2]

Received: 18 March 2016 / Accepted: 12 July 2018 / Published online: 29 August 2018

Abstract
The effects of inclined magnetic field on entropy generation in nanofluid over a stretching sheet were investigated in the presence of partial slip and nonlinear thermal radiation. Applying a similarity variable, the governing equations are reduced to a set of nonlinear ODEs. These equations are solved both analytically and numerically by hypergeometric function and Runge–Kutta Gill method with shooting technique, respectively. For Ag–water, magnetic, aligned angle, nanosolid volume fraction and slip parameters on velocity, temperature, skin friction coefficient and reduced Nusselt number were analyzed. The entropy generation for the influence of the same parameters, radiation parameter and the Reynolds number is discussed for Ag nanoparticles. It is observed that the nanosolid volume fraction and slip parameter reduce the entropy generation. But aligned magnetic field enhances the entropy generation.

Keywords Nanofluid · Aligned magnetic field · Entropy generation · Partial slip · Nonlinear thermal radiation

1 Introduction

The study of magnetohydrodynamic incompressible nanofluid flow has important applications in industrial fields, viz., flow meters, pumps, bearings, the design of heat exchangers and MHD accelerators. The effect of magnetohydrodynamic incompressible nanofluid flow over a semi-infinite vertical plate was numerically investigated by Hamad et al. (2011). MHD three-dimensional flow of an Oldroyd-B nanofluid over a stretching surface, with and without radiation effects was investigated by Shehzad et al. (2016) and Hayat et al. (2015c), respectively. Magnetic field effects in three-dimensional flow of Sisko nanofluid were studied by Hayat et al. (2013, 2016g). Magnetic field effects on viscoelastic nanofluid flow were analyzed by Hayat et al. (2015d) and Farooq et al. (2016). Magnetic field effects on peristaltic copper–water nanofluids were analyzed by Hayat et al. (2016h) and Abbasi et al. (2015). Many of the recent articles are focused on magnetic field effect on the nanofluid flow problems (Hayat et al. 2015a, b, 2016a; Farooq et al. 2015; Hamad 2011; Rahman and Eltayeb 2013; Nadeem et al. 2015).

The presence of entropy generation is used to evaluate loss of energy due to heat transfer and fluid friction irreversibilities. The entropy generation analysis of steady two-dimensional boundary layer nanofluid flow over a flat plate was studied by Malvandi et al. (2013). The numerical solutions of entropy generation analysis for nanofluid flow over a stretching sheet in the presence of partial slip and heat source/sink were presented by Noghrehabadi et al. (2013). The effects of entropy analysis for magnetohydrodynamic nanofluid flow over a permeable stretching surface were reported by Abolbashari et al. (2014). Govindaraju et al. (2015) studied the effect of entropy generation on MHD nanofluid flow over a stretching sheet. Many researchers have discussed the effect of entropy generation on MHD flow with various boundary slip conditions are considered (Das and Jana 2014; Butt et al. 2014; Rashidi et al. 2013).

✉ A. K. Abdul Hakeem
abdulhakeem@rmv.ac.in; abdulhakeem6@gmail.com

[1] Department of Mathematics, Providence College for Women, Coonoor 643 104, India

[2] Department of Mathematics, Sri Ramakrishna Mission Vidyalaya College of Arts and Science, Coimbatore 641 020, India

Rashidi et al. (2014) investigated the radiation effect of water-based nanofluid over a stretching sheet in the presence of magnetic field. The effect of thermal radiation and partial slip on MHD flow in porous medium over a stretching surface were considered by Abdul Hakeem et al. (2014). Hayat et al. (2016b) studied the MHD flow and heat transfer of nanofluids in the presence of nonlinear thermal radiation effects. Shehzad et al. (2014) analyzed the effect of nonlinear thermal radiation in three-dimensional flow of Jeffrey nanofluid. Mushtaq et al. (2014) investigated the nonlinear thermal radiation effects in the laminar two-dimensional flow of nanofluid over a stretching sheet.

The role of the slip boundary condition is vital in some practical situations involving polymer industry, paints, suspensions, foams, polishing of artificial heart valves and circulation of blood. No-slip condition is deficient in such cases. The slip effects of second-grade fluid through a stretching sheet with MHD flow were analyzed by Hayat et al. (2008). The partial slip effects of third-grade fluid through a porous plate were considered by Sajid et al. (2008). The partial slip effects of Oldroyd 8-constant MHD fluid flow over a coaxial cylinders numerically investigated by Khan et al. (2007). The partial slip effects of MHD convective flow due to a rotating disk were examined by Rashidi et al. (2011). Hayat and Mehmood (2011) studied the influence of slip on MHD third order fluid flow in a planar channel. Some recent attempts were described; the slip effects on different fluid flow are presented in Javed et al. (2016), Hayat et al. (2016c, d).

Sulochana et al. (2015) studied the numerical solution of aligned magnetic field and cross-diffusion effects of a nanofluid past an exponentially stretching sheet in porous medium. An analysis has been made both analytically and numerically by Abdul Hakeem et al. (2016) to study the inclined magnetic field effect on the boundary layer flow of a Casson fluid over a stretching sheet. Many of the researchers inclined magnetic field effects on various types of fluid flow were investigated by the followers (Raju et al. 2015; Hayat et al. 2016e).

To the best of author's knowledge so for no one has considered the effects of inclined magnetic field on entropy generation in nanofluid over a stretching sheet. Keeping this in mind, in the present study we have analyzed the effects of inclined magnetic field on entropy generation in nanofluid over a stretching sheet in the presence of radiation and partial slip on both numerically and analytically. The momentum and energy equations are solved; the velocity, temperature, skin friction and the Nusselt number are determined and used to compute the entropy generation. The results are discussed with the help of graphical illustrations and tables.

2 Formulation of the Problem

Consider a steady, laminar, two-dimensional radiative slip flow of an incompressible viscous nanofluid over a stretching sheet in the presence of aligned magnetic field. The velocity of the stretching sheet is $u_{\mathrm{w}} = a\bar{x}$. The temperature at the stretching sheet is deemed to have the constant value T_{w}, while the ambient value, attained as $\bar{y}$ tends to infinity, takes the constant value T_{∞}.

Also consider the aligned magnetic field of uniform strength B_0 which is applied normal to the sheet. It is further assumed that the induced magnetic field is negligible in comparison with the applied magnetic field. The fluid is a water-based nanofluid containing different types of nanoparticles: copper (Cu), silver (Ag), alumina (Al_2O_3) and titanium oxide (TiO_2). It is assumed that the base fluid water and the nanoparticles are in thermal equilibrium and no slip occurs between them. The thermo-physical properties of the nanofluid and the boundary layer equations governing the flow and thermal fields can be written as given by Hamad (2011)

$$\frac{\partial \bar{u}}{\partial \bar{x}} + \frac{\partial \bar{v}}{\partial \bar{y}} = 0 \tag{1}$$

$$\rho_{\mathrm{nf}}\left(\bar{u}\frac{\partial \bar{u}}{\partial \bar{x}} + \bar{v}\frac{\partial \bar{u}}{\partial \bar{y}}\right) = \mu_{\mathrm{nf}}\frac{\partial^2 \bar{u}}{\partial \bar{y}^2} - \sigma B_0^2 \bar{u}\sin^2\gamma \tag{2}$$

$$\left(\rho c_{\mathrm{p}}\right)_{\mathrm{nf}}\left(\bar{u}\frac{\partial T}{\partial \bar{x}} + \bar{v}\frac{\partial T}{\partial \bar{y}}\right) = k_{\mathrm{nf}}\frac{\partial^2 T}{\partial \bar{y}^2} - \frac{\partial q_{\mathrm{r}}}{\partial \bar{y}} \tag{3}$$

where $\bar{x}$ is the coordinate along the sheet, $\bar{u}$ is the velocity components in the $\bar{x}$ direction, $\bar{y}$ is coordinate perpendicular to the sheet, $\bar{v}$ is the velocity component in the $\bar{y}$ direction, T is the local temperature of the fluid, σ is the electric conductivity and q_{r} is the radiative heat flux.

Using Rosseland approximation for radiation (see Hayat et al. 2016f) we have

$$q_{\mathrm{r}} = -\frac{4\sigma^*}{3k^*_{\mathrm{nf}}}\frac{\partial T^4}{\partial \bar{y}} \tag{4}$$

Here, σ^* is the Stefan–Boltzmann constant and k^*_{nf} is the absorption coefficient of the nanofluid. Further, we assume that the temperature difference within the flow is such that T^4 may be expanded in a Taylor series. Hence, expanding T^4 about T_{∞} and neglecting higher-order terms we get,

$$T^4 \cong 4T_{\infty}{}^3 T - 3T_{\infty}{}^4 \tag{5}$$

Substituting Eq. (5) in Eq. (4), (see Hayat et al. 2013) we get

$$q_{\mathrm{r}} = -\frac{16\sigma^* T_{\infty}{}^3}{3k^*_{\mathrm{nf}}}\frac{\partial T}{\partial \bar{y}} \tag{6}$$

Using Eq. (6) in Eq. (3), one obtains

$$\left(\rho c_{\mathrm{p}}\right)_{\mathrm{nf}}\left(\bar{u}\frac{\partial T}{\partial \bar{x}}+\bar{v}\frac{\partial T}{\partial \bar{y}}\right)=k_{\mathrm{nf}}\frac{\partial^2 T}{\partial \bar{y}^2}+\frac{16\sigma^* T_\infty^3}{3k_{\mathrm{nf}}^*}\left(\frac{\partial^2 T}{\partial \bar{y}^2}\right) \tag{7}$$

The effective density of the nanofluid ρ_{nf}, the effective dynamic viscosity of the nanofluid μ_{nf}, the heat capacitance $(\rho C_{\mathrm{p}})_{\mathrm{nf}}$ and the thermal conductivity k_{nf} of the nanofluid are given as

$$\begin{aligned}
&\rho_{\mathrm{nf}}=(1-\phi)\rho_{\mathrm{f}}+\phi\rho_{\mathrm{s}}, && \mu_{\mathrm{nf}}=\frac{\mu_{\mathrm{f}}}{(1-\phi)^{2.5}}\\
&\rho C_{\mathrm{p}})_{\mathrm{nf}}=(1-\phi)(\rho C_{\mathrm{p}})_{\mathrm{f}}+\phi(\rho C_{\mathrm{p}})_{\mathrm{s}}, && k_{\mathrm{nf}}=k_{\mathrm{f}}\left(\frac{k_{\mathrm{s}}+2k_{\mathrm{f}}-2\phi(k_{\mathrm{f}}-k_{\mathrm{s}})}{k_{\mathrm{s}}+2k_{\mathrm{f}}+\phi(k_{\mathrm{f}}-k_{\mathrm{s}})}\right)
\end{aligned} \tag{8}$$

Here, ϕ is the solid volume fraction. The boundary conditions of Eqs. (1)–(3) are

$$\begin{aligned}
&\bar{u}=a\bar{x}+l\frac{\partial \bar{u}}{\partial \bar{y}}, && \bar{v}=v_{\mathrm{w}}, && T=T_{\mathrm{w}} \text{ at } \bar{y}=0\\
&\bar{u}\to 0, && T\to T_\infty && \text{as } \bar{y}\to\infty
\end{aligned} \tag{9}$$

where μ_{f} is the dynamic viscosity of the basic fluid, ρ_{f} and ρ_{s} are the densities of the base fluid and nanoparticle, respectively, $(\rho C_{\mathrm{p}})_{\mathrm{f}}$ and $(\rho C_{\mathrm{p}})_{\mathrm{s}}$ are the specific heat parameters of the base fluid and nanoparticle, respectively, k_{f} and k_{s} are the thermal conductivities of the base fluid and nanoparticle, respectively, and a is constant.

By introducing the following non-dimensional variables

$$\begin{aligned}
&x=\frac{\bar{x}}{\sqrt{\nu_{\mathrm{f}}/a}}, \quad y=\frac{\bar{y}}{\sqrt{\nu_{\mathrm{f}}/a}}, \quad u=\frac{\bar{u}}{\sqrt{a\nu_{\mathrm{f}}}},\\
&v=\frac{\bar{v}}{\sqrt{a\nu_{\mathrm{f}}}}, \quad \theta=\frac{T-T_\infty}{T_{\mathrm{w}}-T_\infty}
\end{aligned} \tag{10}$$

After the non-dimensional form, using the stream function ψ, which is defined as $u=\partial\psi/\partial y$ and $v=-\partial\psi/\partial x$, then system (2) and (7) become

$$\begin{aligned}
&\frac{\partial\psi}{\partial y}\frac{\partial^2\psi}{\partial x\partial y}-\frac{\partial\psi}{\partial x}\frac{\partial^2\psi}{\partial y^2}\\
&=\frac{1}{\left(1-\phi+\phi\frac{\rho_{\mathrm{s}}}{\rho_{\mathrm{f}}}\right)}\left\{\frac{1}{(1-\phi)^{2.5}}\frac{\partial^3\psi}{\partial y^3}-M_n\sin^2\gamma\frac{\partial\psi}{\partial y}\right\}
\end{aligned} \tag{11}$$

$$\begin{aligned}
&\frac{\partial\psi}{\partial y}\frac{\partial\theta}{\partial x}-\frac{\partial\psi}{\partial x}\frac{\partial\theta}{\partial y}\\
&=\frac{1}{(1-\phi+\phi(\rho C_{\mathrm{p}})_{\mathrm{s}}/(\rho C_{\mathrm{p}})_{\mathrm{f}})}\left(1+\frac{4Rd}{3}\right)\frac{1}{Pr}\left(\frac{k_{\mathrm{nf}}}{k_{\mathrm{f}}}\right)\frac{\partial^2\theta}{\partial y^2}
\end{aligned} \tag{12}$$

with the boundary conditions

$$\begin{aligned}
&\frac{\partial\psi}{\partial y}=x+L\frac{\partial^2\psi}{\partial y^2}, && \frac{\partial\psi}{\partial x}=S, && \theta=1 \text{ at } y=0\\
&\frac{\partial\psi}{\partial y}\to 0, && && \theta\to 0 \quad \text{as } y\to\infty
\end{aligned} \tag{13}$$

where $Pr=\frac{\nu_{\mathrm{f}}}{\alpha_{\mathrm{f}}}$ is the Prandtl number, $M_n=\frac{\sigma B_0^2}{a\rho_{\mathrm{f}}}$ is the magnetic parameter and $Rd=\frac{4\sigma^* T_\infty^3}{k_{\mathrm{nf}}k_{\mathrm{nf}}^*}$ is the Radiation parameter.

Now by using the simplified form of Lie-group transformations, namely the scaling group G of transformations (see Hamad 2011), we get the similarity transformations as,

$$\eta=y, \quad \psi=xF(\eta), \quad \theta=\theta(\eta). \tag{14}$$

3 Flow and Thermal Analysis

Now using the similarity transformations (11) and (12), we get

$$\begin{aligned}
&F'''+(1-\phi)^{2.5}\{[1-\phi+\phi(\rho_{\mathrm{s}}/\rho_{\mathrm{f}})]\\
&(FF''-F'^2)-M_nF'\sin^2\gamma\}=0
\end{aligned} \tag{15}$$

$$\theta''+\left(\frac{3}{3+4Rd}\right)\frac{Prk_{\mathrm{f}}[1-\phi+\phi(\rho C_{\mathrm{p}})_{\mathrm{s}}/(\rho C_{\mathrm{p}})_{\mathrm{f}}]}{k_{\mathrm{nf}}}F\theta'=0 \tag{16}$$

where primes denote the differentiation with respect to η. The corresponding boundary conditions become

$$\begin{aligned}
&F(0)=S, \quad F'(0)=1+LF''(0), \quad \theta(0)=1 \text{ at } \eta=0,\\
&F'(\infty)=0, \quad F''(\infty)=0, \quad \theta(\infty)=0 \text{ as } \eta\to\infty
\end{aligned} \tag{17}$$

The exact solution to differential equation (15) satisfying the boundary condition (17) is obtained as (see Abdul Hakeem et al. 2014)

$$F(\eta)=S+X\left(\frac{1-\mathrm{e}^{-m\eta}}{m}\right) \tag{18}$$

where m is the parameter associated with the nanoparticle volume fraction, the magnetic field parameter, slip parameter, suction parameter, the fluid density and the nanoparticle density as follow,Thus, the non-dimensional velocity components are

$$
\begin{aligned}
m &= \frac{-\frac{1}{L\rho_f}0.3333A_5 - \left(0.4199A_7 - \frac{1}{\rho_f^2}A_5^2\right)}{L\left(A_6 + \sqrt{A_6^2 + 4\left(A_7 - \frac{1}{\rho_f^2}A_5^2\right)^3}\right)^{1/3} + \frac{1}{L}\left(0.2646\left(A_6 + \sqrt{A_6^2 + 4\left(A_7 - \frac{1}{\rho_f^2}A_5^2\right)^3}\right)^{1/3}\right)} \\
A_1 &= LS(1-\phi)^{2.5}, \quad A_2 = LMsin^2(\gamma), \quad A_3 = L(1-\phi)^{2.5}, \\
A_4 &= \frac{\rho_s}{\rho^f}, \quad A_5 = \rho_f - A_1\rho_f + A_1\phi\rho_f - A_1\phi\rho_s, \\
A_6 &= -2 + 27LA_3 - 3A_1 + 3A_1^2 + 2A_1^3 - 27LA_3 + 3A_1\phi - 6A_1^2\phi - 6A_1^3\phi + 3A_1^2\phi^2 \\
&\quad + 6A_1^3\phi^2 - 2A_1^3\phi^3 + 18A_2A_3 + 9A_1A_2A_3 - 9A_1A_2A_3\phi + 27LA_3A_4\phi - 3A_1A_4\phi \\
&\quad + 6A_1^2A_4\phi + 6A_1^3A_4\phi - 6A_1^2A_4\phi^2 - 12A_1^3A_4\phi^2 + 6A_1^3A_4\phi^3 + 9A_1A_2A_3A_4\phi \\
&\quad + 3A_1^2A_4^2\phi^2 + 6A_1^3A_4^2\phi^2 - 6A_1^3A_4^2\phi^3 + 2A_1^3A_4^3\phi^3 \\
A_7 &= \frac{1}{\rho_f}(3A_3(-S\rho_f + S\phi\rho_f - A_3\rho_f - S\phi\rho_s)), \quad \text{and} \quad X = \frac{1}{Lm+1}.
\end{aligned} \tag{19}
$$

$$
u = xX\mathrm{e}^{-m\eta}, \quad v = -\left(S + X\left(\frac{1-\mathrm{e}^{-m\eta}}{m}\right)\right) \tag{20}
$$

The dimensional velocity components are

$$
\bar{u} = Xa\bar{x}\mathrm{e}^{-m\sqrt{a/\nu_f}\bar{y}}, \quad \bar{v} = -\left(S + X\left(\frac{1-\mathrm{e}^{-m\sqrt{a/\nu_f}\bar{y}}}{m}\right)\right)\sqrt{a\nu_f} \tag{21}
$$

The shear stress at the stretching sheet characterized by the skin friction coefficient C_f, is given by

$$
C_f = \frac{-2\mu_{nf}}{\rho_f(\overline{u}_w(\bar{x}))^2}\left(\frac{\partial\overline{u}}{\partial\overline{y}}\right)_{\bar{y}=0} \tag{22}
$$

Using Eqs. (10), (14), (18), (19) and (21), the skin friction can be written as

$$
Re_x^{1/2}C_f = -\frac{2}{(1-\phi)^{2.5}}F''(0) \tag{23}
$$

where $Re_x = \bar{x}\bar{u}_w(\bar{x})/\nu_f$ is the local Reynolds number based on the stretching velocity $\bar{u}_w(\bar{x})$. $Re_x^{1/2}C_f$ is the local skin friction coefficient.

4 Analytical Method for Solution

Introducing the new variable,

$$
\xi = -\frac{Prk_f[1-\phi+\phi(\rho C_p)_s/(\rho C_p)_f]}{m^2k_{nf}}\left(\frac{3}{3+4Rd}\right)X\mathrm{e}^{-m\eta} \tag{24}
$$

and inserting (24) in (16), we obtain

$$
\xi\theta_{\xi\xi} + (1-a_0-\xi)\theta_\xi = 0 \tag{25}
$$

and (17) transforms to

$$
\theta\left(-\frac{Pr}{\alpha m^2}\right) = 1 \quad \text{and} \quad \theta(0) = 0 \tag{26}
$$

The solution of Eq. (25) with the corresponding boundary conditions (26), in terms of η is written as

$$
\theta(\eta) = \mathrm{e}^{-ma_0\eta}\frac{M[a_0, a_0+1, -b_0\mathrm{e}^{-m\eta}]}{M[a_0, a_0+1, -b_0]} \tag{27}
$$

where $M[a_0, a_0+1, -b_0\mathrm{e}^{-m\eta}]$ is the Kummer's function, which is given as in Rashidi et al. (2014).

Where

$$
\alpha = \frac{k_{nf}}{k_f(1-\phi+\phi\frac{(\rho C_p)_s}{(\rho C_p)_f})}, \quad a_0 = \frac{Pr}{\alpha}\left(\frac{3}{3+4Rd}\right)\left(\frac{S}{m} + \frac{X}{m^2}\right) \text{ and } b_0 = \frac{Pr}{\alpha m^2}\left(\frac{3}{3+4Rd}\right)X
$$

The quantity of practical interest, in this section the Nusselt number Nu_x which is defined as

$$
Nu_x = \frac{\bar{x}\,\overline{q}_w}{k_f(T_w - T_\infty)}
$$

where $\overline{q}_w = -\left(k_{nf} + \frac{16\sigma T_\infty^3}{3k_{nf}^*}\right)\left(\frac{\partial T}{\partial\bar{y}}\right)_{\bar{y}=0}$ is the local surface heat flux.

We obtain the following Nusselt number

$$
Re_x^{-1/2}Nu_x = \frac{k_{nf}}{k_f}\left(1 + \frac{4Rd}{3}\right)[-\theta'(0)].
$$

The non-dimensional wall temperature gradient derived from Eq. (27) reads as

Table 1 Thermo-physical properties of water and nanoparticles. Reproduced with permission from Hamad (2011)

	ρ (kg/m^3)	C_p (J/kg k)	k (w/mk)	$\beta \times 10^5$ (k^{-1})
Pure water	997.1	4179	0.613	21
Copper (Cu)	8933	385	401	1.67
Silver (Ag)	10,500	235	429	1.89
Alumina (Al_2O_3)	3970	765	40	0.85
Titanium oxide (TiO_2)	4250	686.2	8.9538	0.9

$$\theta'(0) = -ma_0 + \frac{ma_0 b_0}{1+a_0}\frac{M[a_0+1, a_0+2, -b_0]}{M[a_0, a_0+1, -b_0]} \tag{28}$$

5 Numerical Method for Solution

The set of nonlinear ordinary differential equations (15) and (16) with the boundary condition (17) are solved numerically, using Runge–Kutta–Gill method with shooting technique with a systematic guessing of $F_{\eta\eta}(0)$ and $\theta_\eta(0)$. This procedure is repeated until we get the results up to the desired degree of accuracy, namely 10^{-4} with M_n, ϕ, S, L, γ and Rd as prescribed parameters. The code is C++ package, and the numerical solutions are presented in tabular form (Table 1).

6 Entropy Generation Analysis

According to Woods (1975), the local volumetric rate of entropy generation in the presence of magnetic field can be expressed as Woods (1975) and Arpaci (1987)

$$S_G = \frac{k_{nf}}{T_\infty^2}\left[\left(\frac{\partial T}{\partial \bar{x}}\right)^2 + \left(1 + \frac{16\sigma^* T_\infty^3}{3k_{nf}^* k_{nf}}\right)\left(\frac{\partial T}{\partial \bar{y}}\right)^2\right] + \frac{\mu_{nf}}{T_\infty}\left(\frac{\partial \bar{u}}{\partial \bar{y}}\right)^2 + \frac{\sigma B_0^2}{T_\infty}\bar{u}^2 \sin^2\gamma \tag{29}$$

The right hand side of the above equation consists of three parts. The entropy generation due to heat transfer across a finite temperature difference is denoted by the first part, the local entropy generation due to viscous dissipation is denoted by the second part, and the local entropy generation due to the effect of the magnetic field is represented by the third part. The entropy generation number, dimensionless form of entropy generation rate N_S is defined as the ratio of the local volumetric entropy generation rate (S_G) to a characteristic entropy generation rate $(S_G)_0$. For a prescribed boundary condition, the characteristic entropy generation rate is

$$(S_G)_0 = \frac{k_{nf}(\Delta T)^2}{\bar{x}^2 T_\infty^2}; \tag{30}$$

therefore, the entropy generation number is

$$N_s = \frac{S_G}{(S_G)_0} \tag{31}$$

Using Eqs. (27), (29), (30) and (31), the entropy generation number is given by

$$N_s = \left(\frac{3+4Rd}{3}\right)\theta'^2(\eta)Re_x + \frac{Br}{\Omega}F''^2(\eta)Re_x + \frac{BrHa^2}{\Omega}F'^2(\eta)\sin^2\gamma \tag{32}$$

where Br is the Brinkman number. Ω and Ha are, respectively, the dimensionless temperature difference and the Hartmann number. These numbers are given by the following relationships

$$Br = \frac{\mu_{nf}\bar{u}_w^2}{k_{nf}\Delta T}, \quad \Omega = \frac{\Delta T}{T_\infty}, \quad Ha = B_0\bar{x}\sqrt{\frac{\sigma}{\mu_{nf}}} \tag{33}$$

7 Discussion of Results

The velocity, temperature, skin friction, Nusselt number and entropy generation are discussed for inclined magnetic field and other relevant physical parameters graphically for Ag–water. For base fluid water, the Prandtl number is fixed as 6.2. The values of local skin friction coefficient

Table 2 Comparison of results for the reduced Nusselt number $-\theta'(0)$

Pr	Present results		Wang (1989)
	Analytical	Numerical	
0.7	0.4539	0.4539	0.4539
2.0	0.9114	0.9114	0.9114
7.0	1.8954	1.8954	1.8954
20.0	3.3539	3.3539	3.3539

When $\varphi = M_n = Rd = L = S = 0, \gamma = 0^\circ$

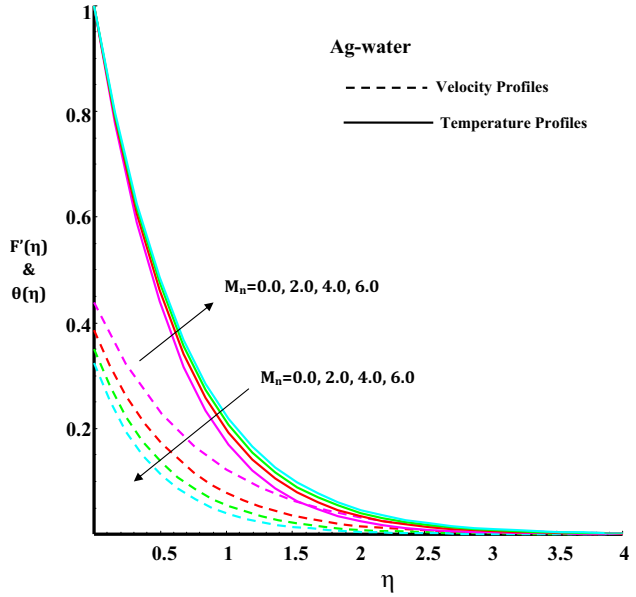

Fig. 1 Effect of magnetic parameter on velocity and temperature distributions with $Pr = 6.2, \phi = 0.1, Rd = 0.5, L = 1.0, \gamma = 45^{\circ}, S = 0.5$

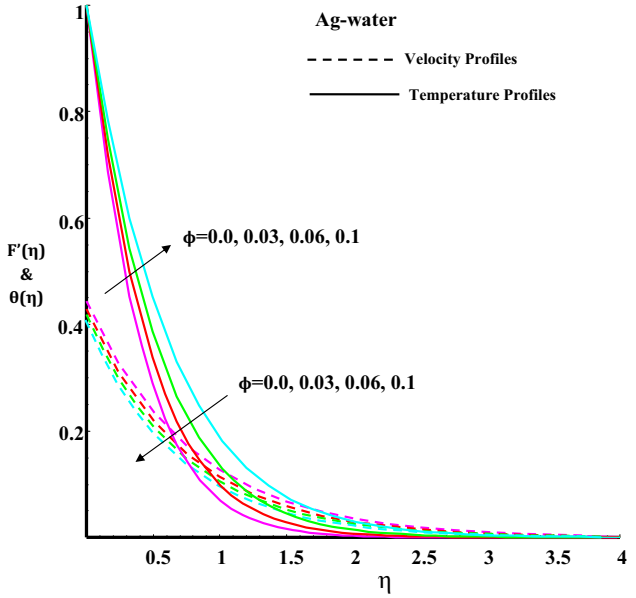

Fig. 3 Effect of nanosolid volume fraction parameter on velocity and temperature distributions with $Pr = 6.2, M_{\mathrm{n}} = 1.0, Rd = 0.5, L = 1.0, \gamma = 45^{\circ}, S = 0.5$

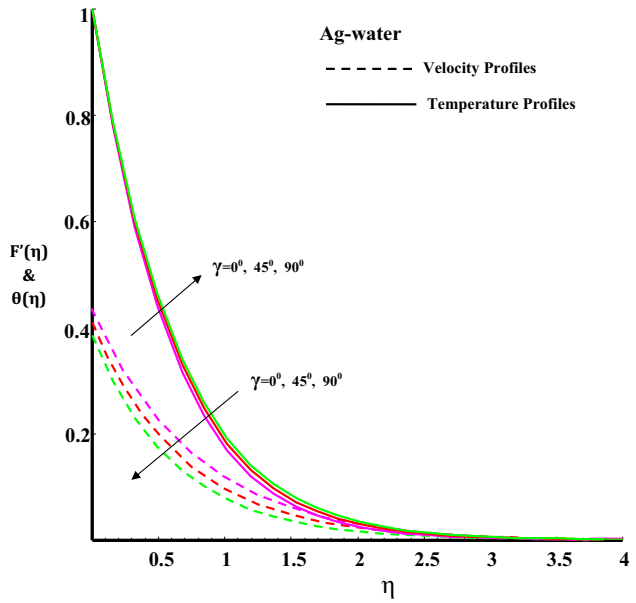

Fig. 2 Effect of angle parameter on velocity and temperature distributions with $Pr = 6.2, M_{\mathrm{n}} = 1.0, \phi = 0.1, Rd = 0.5, S = 0.5, L = 1.0.$

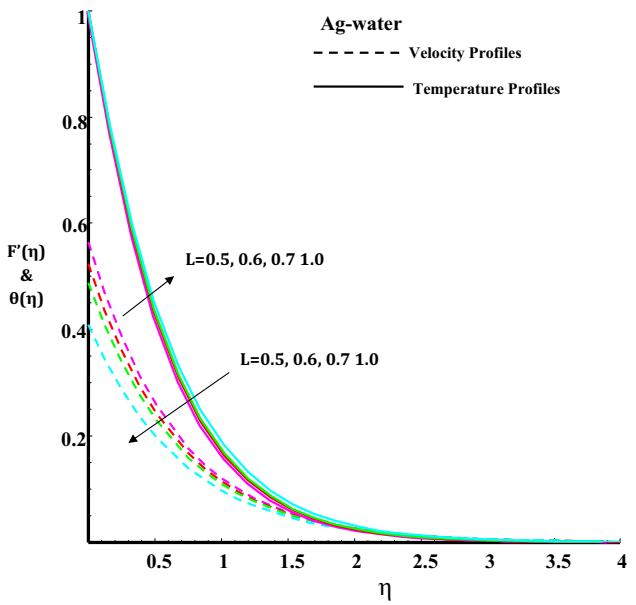

Fig. 4 Effect of the slip parameter on velocity and temperature distribution with $Pr = 6.2, M_{\mathrm{n}} = 1.0, \phi = 0.1, Rd = 1.0, \gamma = 45^{\circ}, S = 0.5$

$Re_x^{-1/2} C_{\mathrm{f}}$ and reduced Nusselt number $Nu_x Re_x^{-1/2}$ are tabulated for different nanoparticles like Cu, Ag, Al_2O_3 and TiO_2. The present results are compared with those of Wang (1989), and an excellent agreement is observed for a special case which is shown in Table 2.

Figures 1 and 2 depict the behavior of the velocity and temperature profiles for various values of magnetic parameter and aligned angle, respectively. It is evident from the figures that an increase in the magnetic parameter and aligned angle cases decreases the momentum boundary layer and increases the thermal boundary layer. The magnetic field effect is negligible in the case of $\gamma = 0^{\circ}$, and transverse magnetic field effect is presented in the case of $\gamma = 90^{\circ}$. The enhanced aligned angle ($0^{\circ}-90^{\circ}$) strengthens the applied magnetic field; strengthening the magnetic field causes to develop the force opposite to the flow which is

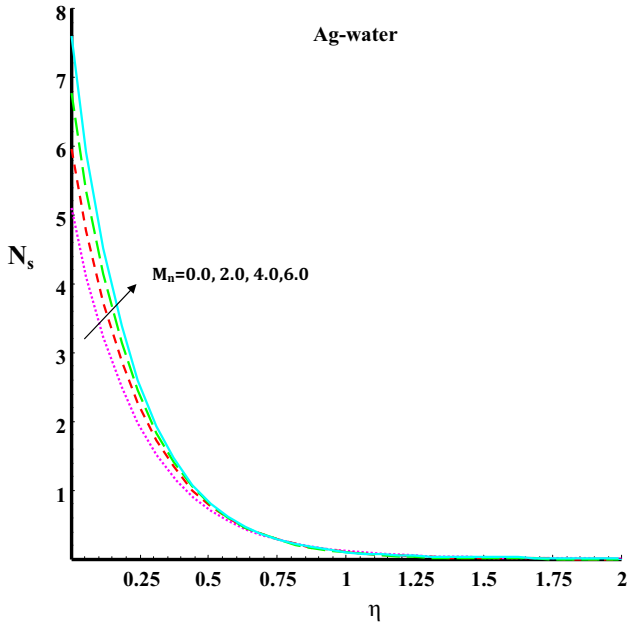

Fig. 5 Effect of magnetic parameter on entropy generation with $Pr = 6.2, \phi = 0.1, Rd = 0.5, L = 0.01, \gamma = 45°, S = 0.5, Br\,\Omega^{-1} = 1.0, zRe_x = 1.0, Ha = 1.0$

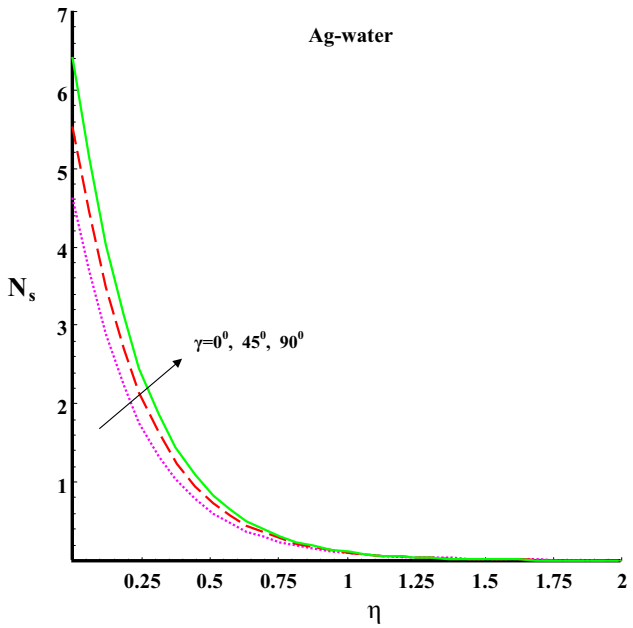

Fig. 6 Effect of angle parameter on entropy generation with $Pr = 6.2, M_n = 1.0, \phi = 0.1, Rd = 0.5, L = 0.01, S = 0.5, Br\,\Omega^{-1} = 1.0, Re_x = 1.0, Ha = 1.0$

called Lorentz force. This can be concluded by the fact that the increase in the aligned magnetic field reduces the motion of the nanofluid velocity and enhances the temperature of the nanofluid.

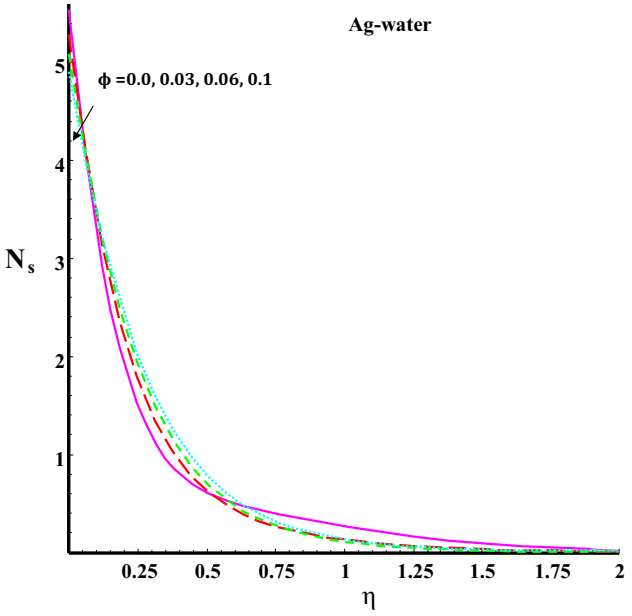

Fig. 7 Effect of nanosolid volume fraction parameter on entropy generation with $Pr = 6.2, M_n = 1.0, Rd = 0.7, L = 0.01, \gamma = 45°, S = 0.5, Br\,\Omega^{-1} = 1.0, Re_x = 1.0, Ha = 1.0$

Effects of nanosolid volume fraction parameter on velocity and temperature profiles are presented in Fig. 3. It can be seen that nanosolid volume fraction parameter increases as the velocity of the nanofluid motion is slowed down. Further, the presence of silver nanoparticle enhances with the temperature profile. This is because silver particles have high thermal conductivity, so the thermal boundary layer thickness increases.

Figure 4 illustrates the effect of slip parameter on velocity and temperature profiles. This reveals that, the velocity increases, as the slip parameter decreases. Because in this case slip occurs, the flow velocity near the sheet will not be equal to the stretching velocity of the sheet. With the increase in slip parameter, the slip velocity increases and consequently nanofluid velocity decreases. Also, this is due to the fact that the temperature increases as increasing the slip parameter.

The effects of magnetic parameter and aligned angle on entropy generation profiles are shown in Figs. 5 and 6, respectively. These figures reveal that an increase in both magnetic parameter and aligned angle enhances the entropy generation. The influence of aligned magnetic field creates more entropy in nanofluid flow, indicating that the surface acts as the strong source of irreversibility and randomness generation.

Figure 7 exhibits the effect of nanosolid volume fraction on entropy generation. As the volume of silver nanoparticle increases, the entropy generation decreases. It is found that

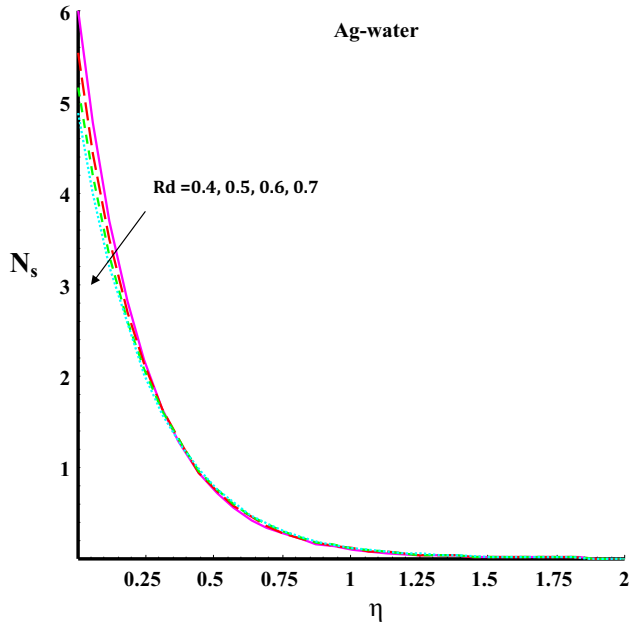

Fig. 8 Effect of Radiation parameter on entropy generation with $Pr = 6.2, M_n = 1.0, \phi = 0.1, L = 0.01, \gamma = 45^\circ, S = 0.5, Re_x = 1.0, Ha = 1.0$

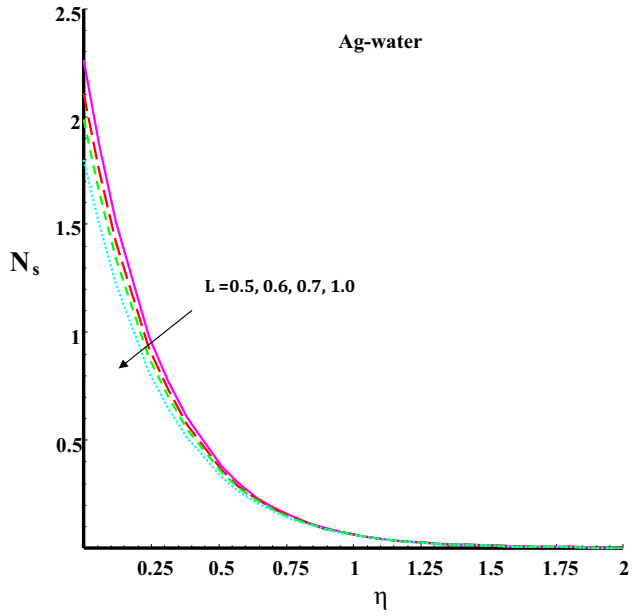

Fig. 9 Effect of slip parameter on entropy generation with $Pr = 6.2, M_n = 1.0, \phi = 0.1, Rd = 0.5, S = 0.5, \gamma = 45^\circ, Br\,\Omega^{-1} = 1.0, Re_x = 1.0, Ha = 1.0$

the entropy generation decreases with the increasing values of nanosolid volume fraction due to the higher dissipation energy resulted from the sharper velocity gradient near the wall and opposite behavior is observed far away from the wall.

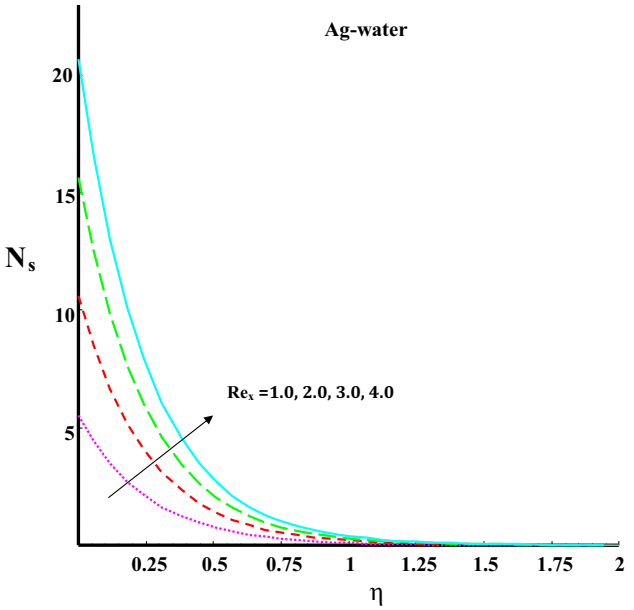

Fig. 10 Effect of Reynolds number on entropy generation with $Pr = 6.2, M_n = 1.0, \phi = 0.1, Rd = 0.5, L = 0.01, \gamma = 45^\circ, Br\,\Omega^{-1} = 1.0, S = 0.5$

The effect of radiation parameter on entropy generation is shown in Fig. 8. It is observed that radiation parameter increases when entropy generation decreases. This is because, the transfer of heat energy is observed the entropy production.

Figure 9 displays the distinction of entropy generation for different values of slip parameter. As the value of slip parameter increases, the entropy generation decreases. The entropy generation profiles for various values of Reynolds number are shown in Fig. 10. It is observed that the entropy generation increases with the increasing values of Reynolds number.

The skin friction coefficient $-f''(0)$ against magnetic parameter for various values of slip parameter, aligned angle parameter, nanosolid volume fraction parameter and suction parameters is shown in Fig. 11a, b, respectively. Figure 11a shows that $-f''(0)$ increases with aligned angle parameter, while it decreases with an increase in slip parameter. Figure 11b reveals that $-f''(0)$ increases with increasing nanosolid volume fraction parameter and suction parameter. The variation of reduced Nusselt number $-\theta'(0)$ against magnetic parameter for various values of slip parameter, aligned angle parameter, nanosolid volume fraction parameter, suction parameter and radiation parameter is shown in Fig. 12a, b. Figure 12a illustrates, $-\theta'(0)$ increases with decreasing value of slip parameter

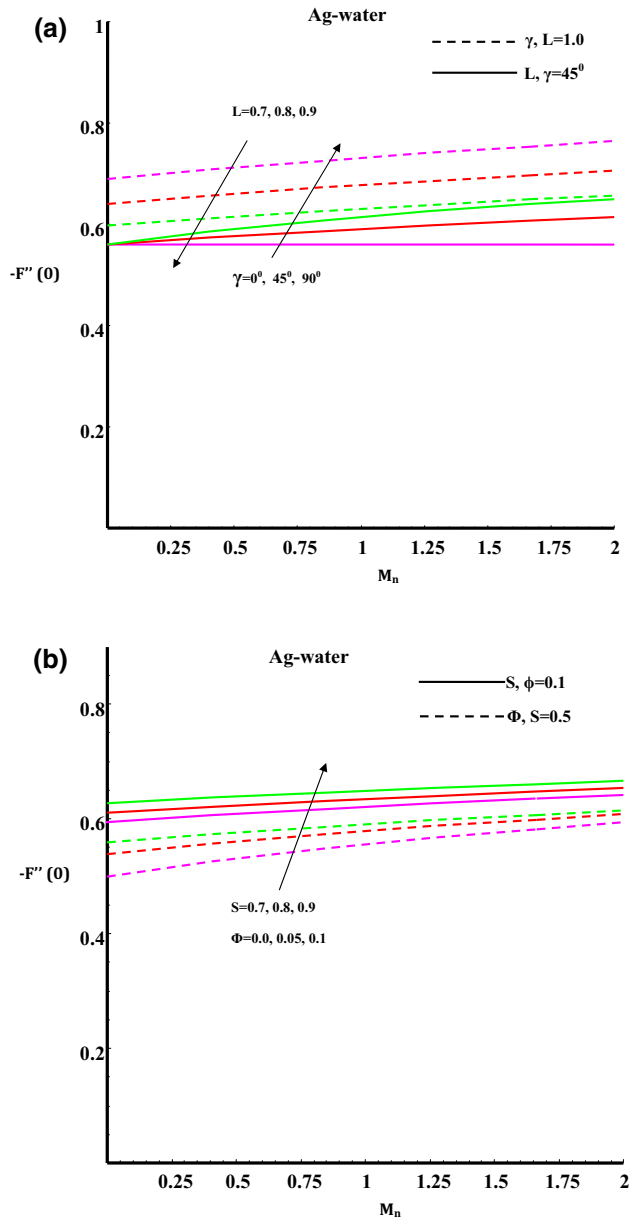

Fig. 11 **a** Variation of the skin friction coefficient with respect to magnetic parameter for slip parameter and angle parameter when $Pr = 6.2, \phi = 0.1, S = 0.5$. **b** Variation of the skin friction coefficient with respect to magnetic parameter for nanosolid volume fraction parameter and suction parameter when $Pr = 6.2, L = 1.0, \gamma = 45^{\circ}$

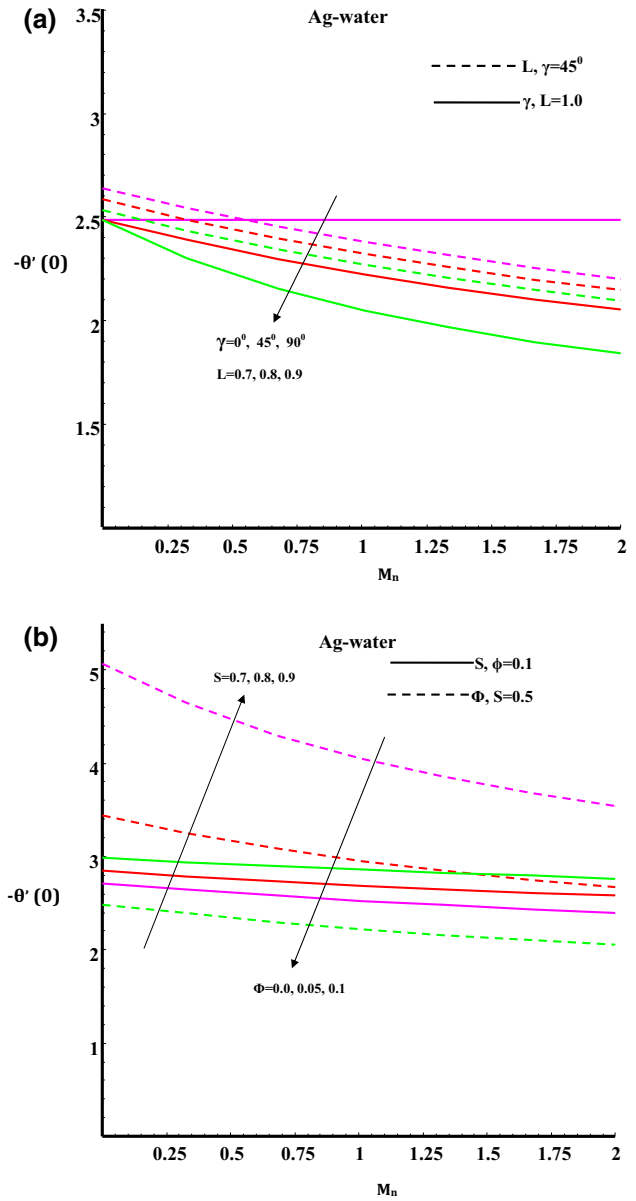

Fig. 12 **a** Variation of the Nusselt number with respect to magnetic parameter for slip parameter and angle parameter when $Pr = 6.2, Rd = 0.5, S = 0.5, \phi = 0.1$. **b** Variation of the Nusselt number with respect to magnetic parameter for nanosolid volume fraction parameter and suction parameter when $Pr = 6.2, L = 1.0, Rd = 0.5, \gamma = 45^{\circ}$

and aligned angle parameter. Figure 12b reveals that $-\theta'(0)$ increases with increasing value of suction parameter and it decreases with increasing value of nanosolid volume fraction.

Tables 3 and 4 reveal the values of local skin friction coefficient and the reduced Nusselt number for different nanoparticles such as Cu, Ag, Al_2O_3 and TiO_2. From these tables, it shows that the skin friction increases with M_n, γ and S and decreases with L. It is also observed that the increasing values of ϕ increase the skin friction coefficient of metallic nanofluids (Ag–water and Cu–water) and it has an opposite effect on nonmetallic nanofluids (Al_2O_3–water and TiO_2–water). The reduced Nusselt number increases with Rd and S and decreases with M_n, γ, ϕ and L. This result shows that the reduced Nusselt number of metallic nanofluids is lower than nonmetallic nanofluids.

Table 3 Values of $-F''(0)$ for various of the parameter

Parameters	Values	Cu		Ag		Al_2O_3		TiO_2	
		Analytical	Numerical	Analytical	Numerical	Analytical	Numerical	Analytical	Numerical
M_n	0.0	0.547029	0.547029	0.559587	0.559587	0.499649	0.499649	0.502710	0.502710
	2.0	0.606464	0.606464	0.614623	0.614623	0.577746	0.577746	0.579500	0.579500
	4.0	0.644161	0.644161	0.650263	0.650263	0.623306	0.623306	0.624550	0.624550
γ	0°	0.547029	0.547029	0.559587	0.559587	0.499649	0.499649	0.502710	0.502710
	45°	0.580735	0.580735	0.590605	0.590605	0.545079	0.545079	0.547301	0.547301
	90°	0.606464	0.606464	0.614623	0.614623	0.577746	0.577746	0.579500	0.579500
φ	0.0	0.556178	0.556178	0.556178	0.556178	0.556178	0.556178	0.556178	0.556178
	0.05	0.572141	0.572141	0.578109	0.578109	0.551739	0.551739	0.552957	0.552957
	0.1	0.580735	0.580735	0.590605	0.590605	0.545079	0.545079	0.547301	0.547301
L	0.7	0.716262	0.716262	0.730935	0.730935	0.663695	0.663695	0.666952	0.666952
	0.8	0.664217	0.664217	0.676937	0.676937	0.618497	0.618497	0.621337	0.621337
	1.0	0.580735	0.580735	0.590605	0.590605	0.545079	0.545079	0.547301	0.547301
S	0.6	0.595087	0.595087	0.605668	0.605668	0.556794	0.556794	0.559183	0.559183
	0.7	0.609161	0.609161	0.620387	0.620387	0.568398	0.568398	0.570946	0.570946
	0.8	0.622886	0.622886	0.634684	0.634684	0.579852	0.579852	0.582549	0.582549

While studying the effect of individual parameters, the following values are assumed $Pr = 6.2, M_n = 1.0, \varphi = 0.1, \gamma = 45°, L = 1.0$ and $S = 0.5$

Table 4 Values of $-\theta'(0)$ for various of the parameter

Parameters	Values	Cu		Ag		Al_2O_3		TiO_2	
		Analytical	Numerical	Analytical	Numerical	Analytical	Numerical	Analytical	Numerical
M_n	0.0	0.798052	0.798052	0.769466	0.769466	0.847814	0.847814	0.884295	0.884295
	2.0	0.742994	0.742994	0.719442	0.719442	0.773999	0.773999	0.810400	0.810400
	4.0	0.709948	0.709948	0.688936	0.688936	0.732587	0.732587	0.768540	0.768540
γ	0°	0.798052	0.798052	0.769466	0.769466	0.847814	0.847814	0.884295	0.884295
	45°	0.766508	0.766508	0.740935	0.740935	0.804695	0.804695	0.841239	0.841239
	90°	0.742994	0.742994	0.719442	0.719442	0.773999	0.773999	0.810400	0.810400
φ	0.0	1.146350	1.146350	1.146350	1.146350	1.146350	1.146350	1.146350	1.146350
	0.05	0.937285	0.937285	0.921373	0.921373	0.960650	0.960650	0.981660	0.981660
	0.1	0.766508	0.766508	0.740935	0.740935	0.804695	0.804695	0.841239	0.841239
L	0.7	0.796823	0.796823	0.770173	0.770173	0.837120	0.837120	0.874635	0.874635
	0.8	0.785588	0.785588	0.759318	0.759318	0.825183	0.825183	0.862335	0.862335
	1.0	0.766508	0.766508	0.740935	0.740935	0.804695	0.804695	0.841239	0.841239
S	0.6	0.855535	0.855535	0.827775	0.827775	0.894402	0.894402	0.936114	0.936114
	0.7	0.947154	0.947154	0.917231	0.917231	0.986443	0.986443	1.033470	1.033470
	0.8	1.041060	1.041060	1.009000	1.009000	1.080550	1.080550	1.133020	1.133020
Rd	0.5	0.766508	0.766508	0.740935	0.740935	0.804695	0.804695	0.841239	0.841239
	0.6	0.861394	0.861394	0.833344	0.833344	0.901787	0.901787	0.942764	0.942764
	1.0	1.151110	1.151110	1.115800	1.115800	1.197120	1.197120	1.251770	1.251770

While studying the effect of individual parameters, the following values are assumed $Pr = 6.2, M_n = 1.0, \varphi = 0.1, Rd = 0.5, \gamma = 45°, L = 1.0,$ and $S = 0.5$

8 Conclusion

This article gives the analytical and numerical solutions of inclined magnetic field on entropy generation in nanofluid flow over a stretching sheet in the presence of partial slip and nonlinear thermal radiation. The velocity and temperature profiles are obtained and used to compute the entropy generation. The main conclusions derived from this study are as follows.

- The velocity of the nanofluid decreases with the increasing magnetic parameter, aligned angle, nanosolid volume fraction parameter and slip parameter.
- The temperature of the nanofluid increases with the increasing values of magnetic parameter, aligned angle, nanosolid volume fraction parameter, slip parameters.
- The increasing values of magnetic parameter, aligned angle and Reynolds number increase the generation of entropy in the nanofluid flow field. The entropy generation increases with decrease in nanosolid volume fraction parameter, radiation parameter and slip parameter.

Acknowledgements One of the authors (A. K. Abdul Hakeem) gratefully acknowledges the financial support of minor research project, UGC, New Delhi, India under UGC/SERO/MRP-6729/16 for pursuing this work.

References

Abbasi FM, Hayat T, Alsaedi A (2015) Peristaltic transport of magneto-nanoparticles submerged in water: model for drug delivery system. Phys E 66:123–132

Abdul Hakeem AK, Kalaivanan R, Vishnu Ganesh N, Ganga B (2014) Effect of partial slip on hydromagnetic flow over a porous stretching sheet with non-uniform heat source/sink, thermal radiation and wall mass transfer. Ain Shams Eng J 5:913–922

Abdul Hakeem AK, Renuka P, Vishnu Ganesh N, Kalaivanan R, Ganga B (2016) Influence of inclined Lorentz forces on boundary layer flow of Casson fluid over an impermeable stretching sheet with heat transfer. J Magn Magn Mater 401:354–361

Abolbashari MH, Freidoonimehr N, Nazari F, Rashidi MM (2014) Entropy analysis for an unsteady MHD flow past a stretching permeable surface in nanofluid. Power Technol 267:256–267

Arpaci VS (1987) Radiative entropy production-lost heat into entropy. Int J Heat Mass Transf 30:2115–2123

Butt AS, Ali A, Mehmood A (2014) Irreversibility analysis of magnetohydrodynamic flow over a stretching sheet with partial slip and convective boundary. Int J Phys Sci 4:046–060

Das S, Jana RN (2014) Entropy generation due to MHD flow in a porous channel with Navier slip. Ain Shams Eng J 5:575–584

Farooq U, Zhao YL, Hayat T, Alsaedi A, Liao SJ (2015) Application of the HAM-based Mathematica package BVPh 2.0 on MHD Falkner–Skan flow of nano-fluid. Comput Fluids 111:69–75

Farooq M, Ijaz Khan M, Waqas M, Hayat T, Alsaedi A, Imran Khan M (2016) MHD stagnation point flow of viscoelastic nanofluid with non-linear radiation effects. J Mol Liq 221:1097–1103

Govindaraju M, Vishnu Ganesh N, Ganga B, Abdul Hakeem AK (2015) Entropy generation analysis of magneto hydrodynamic flow of a nanofluid over a stretching sheet. J Egypt Math Soc 23:426–434

Hamad MAA (2011) Analytical solution of natural convection flow of a nanofluid over a linearly stretching sheet in the presence of magnetic field. Int Commun Heat Mass Transf 38:487–492

Hamad MAA, Pop I, Md Ismil AI (2011) Magnetic field effects on free convection flow of a nanofluid past a vertical semi-infinite flat plate. Nonlinear Anal Real 12:1338–1346

Hayat T, Mehmood OU (2011) Slip effects on MHD flow of third order fluid in a planar channel. Commun Nonlinear Sci Numer Simulat 16:1363–1377

Hayat T, Javed T, Abbas Z (2008) Slip flow and heat transfer of a second grade fluid past a stretching sheet through a porous space. Int J Heat Mass Transf 51:4528–4534

Hayat T, Muhammad T, Ahmad B, Shehzad SA (2013) Impact of magnetic field in three-dimensional flow of Sisko nanofluid with convective condition. J Magn Magn Mater 413:1–8

Hayat T, Muhammad T, Shehzad SA, Chen GQ, Ibrahim Abbas A (2015a) Interaction of magnetic field in flow of Maxwell nanofluid with convective effect. J Magn Magn Mater 389:48–55

Hayat T, Imtiaz M, Alsaedi A, Marwan Kutbi A (2015b) MHD three-dimensional flow of nanofluid with velocity slip and nonlinear thermal radiation. J Magn Magn Mater 396:31–37

Hayat T, Muhammad T, Shehzad SA, Alhuthali MS, Jinhu L (2015c) Impact of magnetic field in three-dimensional flow of an Oldroyd-B nanofluid. J Mol Liq 212:272–282

Hayat T, Muhammad T, Alsaedi A, Alhuthali MS (2015d) Magnetohydrodynamic three-dimensional flow of viscoelastic nanofluid in the presence of nonlinear thermal radiation. J Magn Magn Mater 385:222–229

Hayat T, Muhammad T, Qayyum A, Alsaedi A, Mustafa M (2016a) On squeezing flow of nanofluid in the presence of magnetic field effects. J Mol Liq 213:179–185

Hayat T, Qayyum S, Imtiaz M, Alsaedi A (2016b) Comparative study of silver and copper water nanofluids with mixed convection and nonlinear thermal radiation. Int J Heat Mass Transf 102:723–732

Hayat T, Shafique M, Tanveer A, Alsaedi A (2016c) Hall and ion slip effects on peristaltic flow of Jeffrey nanofluid with Joule heating. J Magn Magn Mater 407:51–59

Hayat T, Qayyum S, Imtiaz M, Alzahrani F, Alsaedi A (2016d) Partial slip effect in flow of magnetite-Fe_3O_4 nanoparticles between rotating stretchable disks. J Magn Magn Mater 413:39–48

Hayat T, Bibi S, Rafiq M, Alsaedi A, Abbasi FM (2016e) Effect of an inclined magnetic field on peristaltic flow of Williamson fluid in an inclined channel with convective conditions. J Magn Magn Mater 401:733–745

Hayat T, Qayyum S, Alsaedi A, Shafique M (2016f) Inclined magnetic field and heat source/sink aspects in flow of nanofluid with nonlinear thermal radiation. Int J Heat Mass Transf 103:99–107

Hayat T, Muhammad T, Shehzad SA, Alsaedi A (2016g) On three-dimensional boundary layer flow of Sisko nanofluid with magnetic field effects. Adv Powder Technol 27:504–512

Hayat T, Farooq S, Alsaedi A, Ahmad B (2016h) Influence of variable viscosity and radial magnetic field on peristalsis of copper–water nanomaterial in a non-uniform porous medium. Int J Heat Mass Transf 103:1133–1143

Javed M, Hayat T, Mustafa M, Ahmad B (2016) Velocity and thermal slip effects on peristaltic motion of Walters-B fluid. Int J Heat Mass Transf 96:210–217

Khan K, Hayat T, Ayub M (2007) Numerical study of partial slip on the MHD flow of an Oldroyd 8-constant fluid. Comput Math Appl 53:1088–1097

Malvandi A, Ganji DD, Hedayati F, Yousefi Rad E (2013) An analytical study on entropy generation of nanofluids over a flat plate. Alex Eng J 52:595–604

Mushtaq A, Mustafa M, Hayat T, Alsaedi A (2014) Nonlinear radiative heat transfer in the flow of nanofluid due to solar energy: a numerical study. J Taiwan Inst Chem Eng 45:1176–1183

Nadeem S, Mehmood R, Motsa SS (2015) Numerical investigation on MHD oblique flow of a Walter's B type nanofluid over a convective surface. Int J Therm Sci 92:162–172

Noghrehabadi A, Saffarian MR, Pourrajab R, Ghalambaz M (2013) Entropy analysis for nanofluid flow over a stretching sheet in the presence of heat generation/absorption and partial slip. J Mech Sci Technol 27:927–937

Rahman MM, Eltayeb IA (2013) Radiative heat transfer in a hydromagnetic nanofluid past a nonlinear stretching surface with convective boundary condition. Meccanica 48:601–615

Raju CSK, Sandeep N, Sulochana C, Sugunamma V, Jayachandra Babu M (2015) Radiation, inclined magnetic field and cross-diffusion effects on flow over a stretching surface. J Niger Math Soc 34:169–180

Rashidi MM, Hayat T, Erfani E, Mohimanian Pour SA, Awatif Hendi A (2011) Simultaneous effects of partial slip and thermal-diffusion and diffusion-thermo on steady MHD convective flow due to a rotating disk. Commun Nonlinear Sci Numer Simul 16:4303–4317

Rashidi MM, Abelman S, Freidooni Mehr N (2013) Entropy generation in steady MHD flow due to a rotating porous disk in a nanofluid. Int J Heat Mass Transf 62:515–525

Rashidi MM, Vishnu Ganesh N, Abdul Hakeem AK, Ganga B (2014) Buoyancy effect on MHD flow of nanofluid over a stretching sheet in the presence of thermal radiation. J Mol Liq 198:234–238

Sajid M, Mahmood R, Hayat T (2008) Finite element solution for flow of a third grade fluid past a horizontal porous plate with partial slip. Comput Math Appl 56:1236–1244

Shehzad SA, Hayat T, Alsaedi A, Obid MA (2014) Nonlinear thermal radiation in three-dimensional flow of Jeffrey nanofluid: a model for solar energy. Appl Math Comput 248:273–286

Shehzad SA, Abdullah Z, Abbasi FM, Hayat T, Alsaedi A (2016) Magnetic field effect in three-dimensional flow of an Oldroyd-B nanofluid over a radiative surface. J Magn Magn Mater 399:97–108

Sulochana C, Sndeep N, Sugunamma V, Rushi Kumar B (2015) Aligned magnetic field and cross-diffusion effects of a nanofluid over an exponentially stretching surface in porous medium. Appl Nanosci. https://doi.org/10.1007/s13204-015-0475-x

Wang CY (1989) Free convection on a vertical stretching surface. J Appl Math Mech (ZAMM) 69:418–420

Woods LC (1975) Thermodynamics of fluid systems. Oxford University Press, Oxford